Supplementary Information for:

Vanadium Pyridonates: Dimerization, Redox Behaviour, and Metal-Ligand Cooperativity

Samuel E. Griffin, Olivia V. Adamczyk, and Laurel L. Schafer*

Department of Chemistry, University of British Columbia, 2036 Main Mall, Vancouver, British Columbia, Canada V6T 1Z1

Table of Contents

NMR Reactions
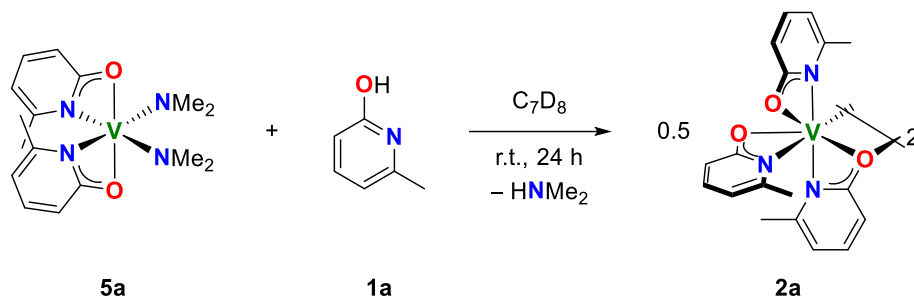
Reduction of 5a to 2a on NMR scale: Complex **5a** (0.003 g, 0.009 mmol) was first weighed into a small vial and then quantitatively transferred to a J. Young tube using ~0.75 mL C_7D_8, giving a crimson solution. A t = 0 ^{1}H NMR spectrum was then obtained before pyridone **1a** (0.001 g, 0.009 mmol) was transferred to the J. Young tube using ~0.4 mL C_7D_8; the colour took on a slight brown hue. The tube was then continuously inverted at room temperature for 24 h and periodically monitored by ^{1}H NMR spectroscopy, during which time the solution became orange-yellow in colour. After 24 h, the signals due to pyridone **1a** had disappeared from the ^{1}H NMR spectrum and signals matching that of isolated complex **2a** were observed.[1]
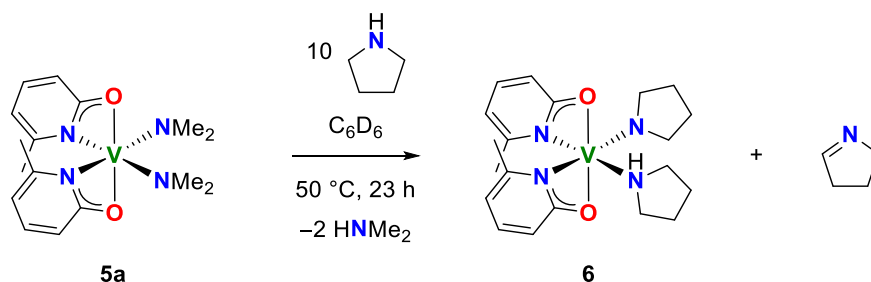
Reduction of 5a to 6 on NMR scale: Complex **5a** (0.005 g, 0.01 mmol) was first weighed into a small vial and then quantitatively transferred to a J. Young tube using ~0.5 mL C_6D_6, giving a crimson solution. A t = 0 ^{1}H NMR spectrum was then obtained before pyrrolidine (0.010 g, 0.14 mmol) was transferred to the J. Young tube using ~0.3 mL C_6D_6; no colour change was observed. Once again, a ^{1}H NMR spectrum was obtained, showing little change beyond the new signals of pyrrolidine. The tube was then heated to 50 °C for 23 h. After the reaction, the solution had become a lighter red-orange colour. Another ^{1}H NMR spectrum was then obtained, showing signals matching that of isolated complex **6** and confirming the formation of pyrroline as a byproduct.[2]

NMR Spectra

Figure S1. ^{1}H NMR spectrum of **2a** *in situ* (C$_7$D$_8$, 300 MHz, 298 K).[1] Broadened resonances result from the paramagnetic V centre.
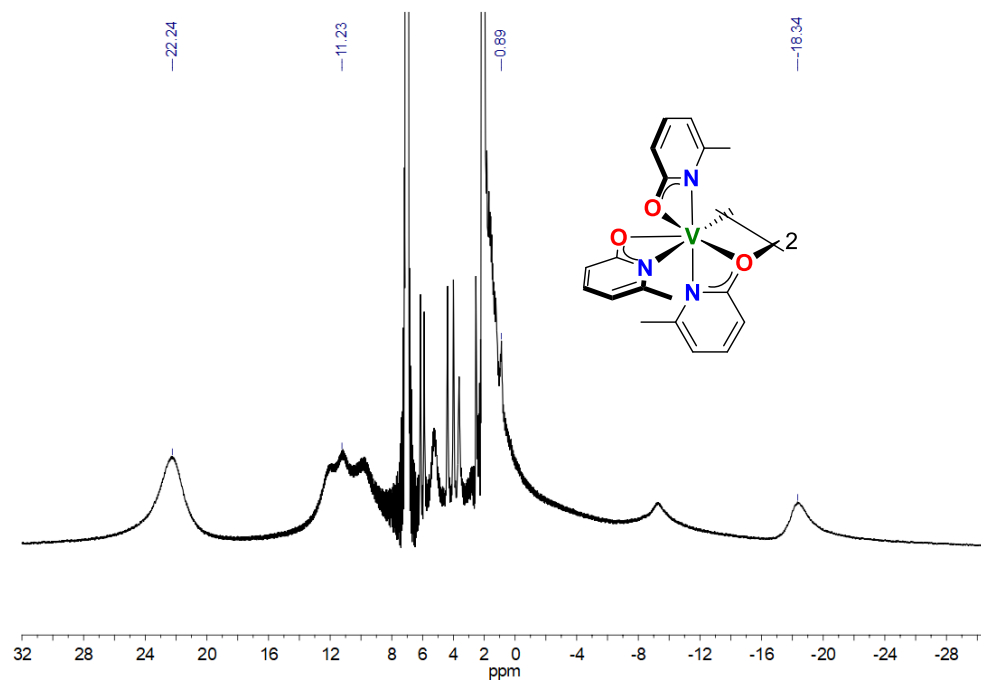
Figure S2. ^{1}H NMR spectrum of **4** and cyclooctane (C$_6$D$_6$, 400 MHz, 298 K). Broadened resonances result from the paramagnetic V centre.
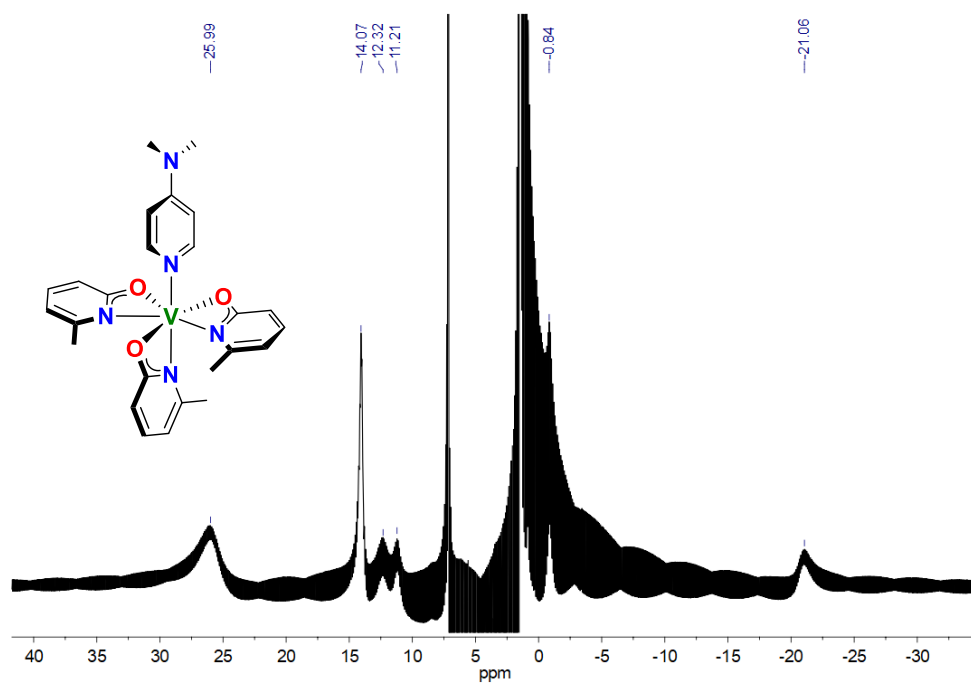
Figure S3. ^{1}H NMR spectrum of **5a** (C_6D_6, 300 MHz, 298 K). Broadened resonances result from the paramagnetic V centre.
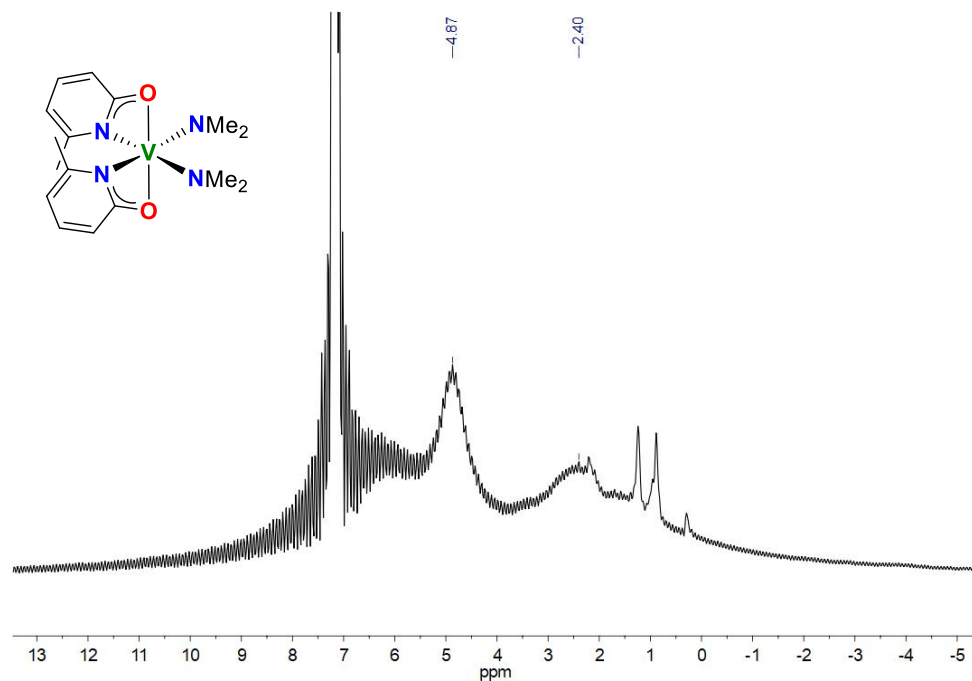
Figure S4. ^{1}H NMR spectrum of **5b** (C_6D_6, 300 MHz, 298 K). Broadened resonances result from the paramagnetic V centre.
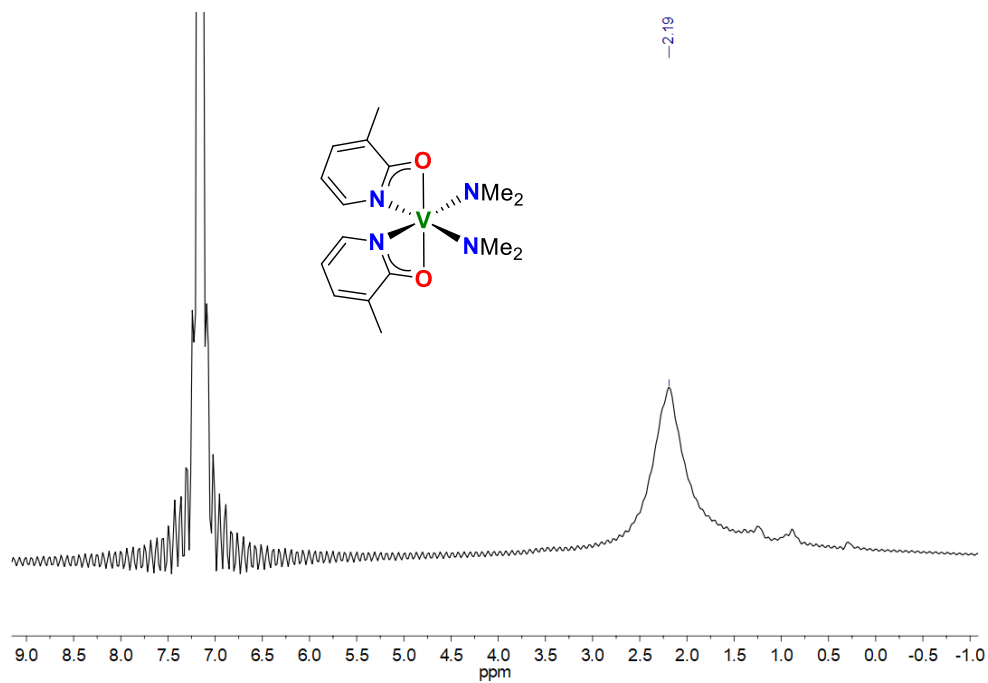
Figure S5. ^{1}H NMR spectrum of **5c** (C_6D_6, 300 MHz, 298 K). Broadened resonances result from the paramagnetic V centre.
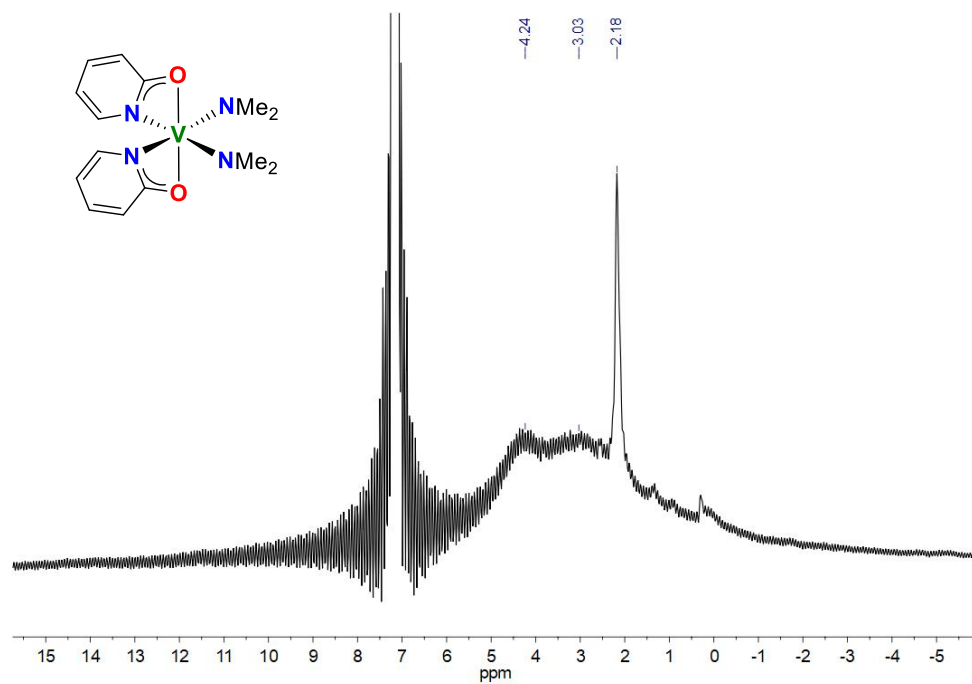
Figure S6. ^{1}H NMR spectrum of **6** (C_6D_6, 300 MHz, 298 K). Broadened resonances result from the paramagnetic V centre.
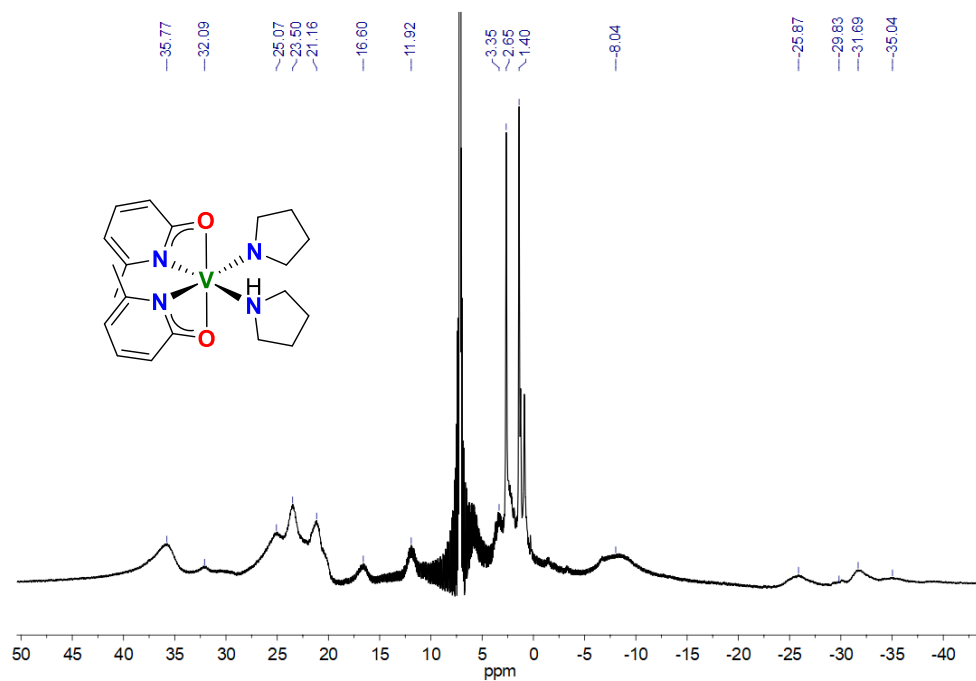
Figure S7. ^{1}H NMR spectrum of **9** (C$_6$D$_6$, 300 MHz, 298 K). Broadened resonances result from the paramagnetic V centre.
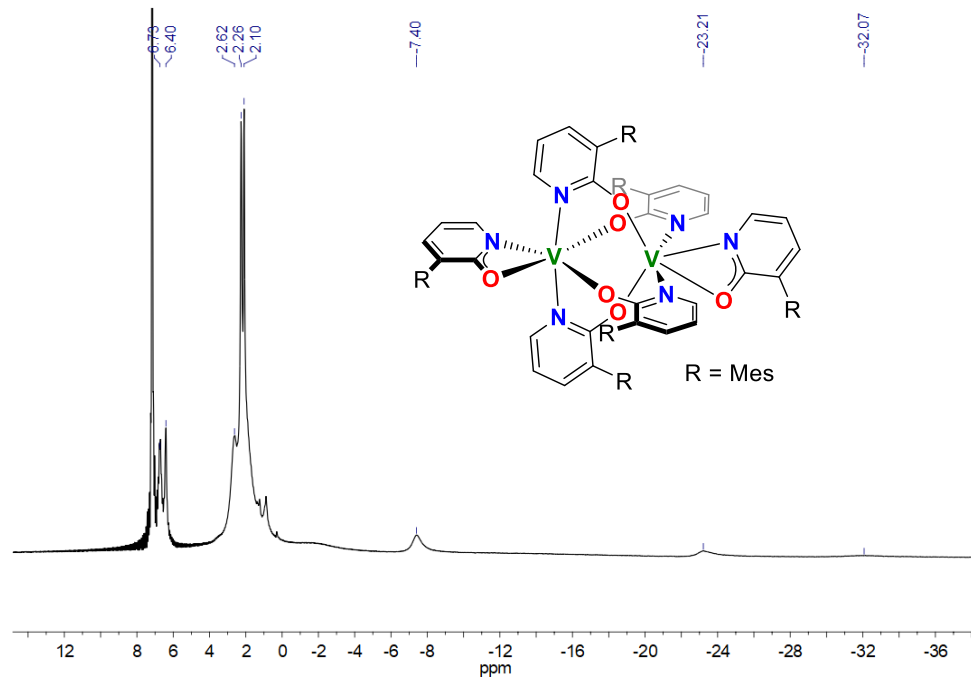
Figure S8. ^{1}H NMR spectrum of **11** (C$_6$D$_6$, 300 MHz, 298 K). Broadened resonances result from the paramagnetic V centre.
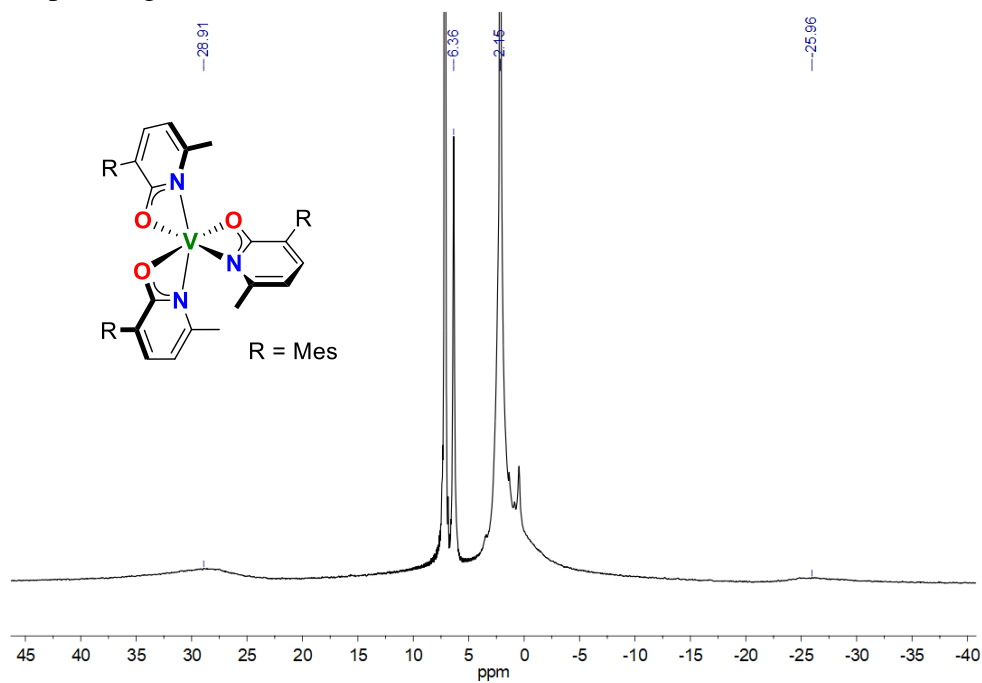
Figure S9. ^{1}H NMR spectrum of **13** (C$_6$D$_6$, 300 MHz, 298 K). Broadened resonances result from the paramagnetic V centre.
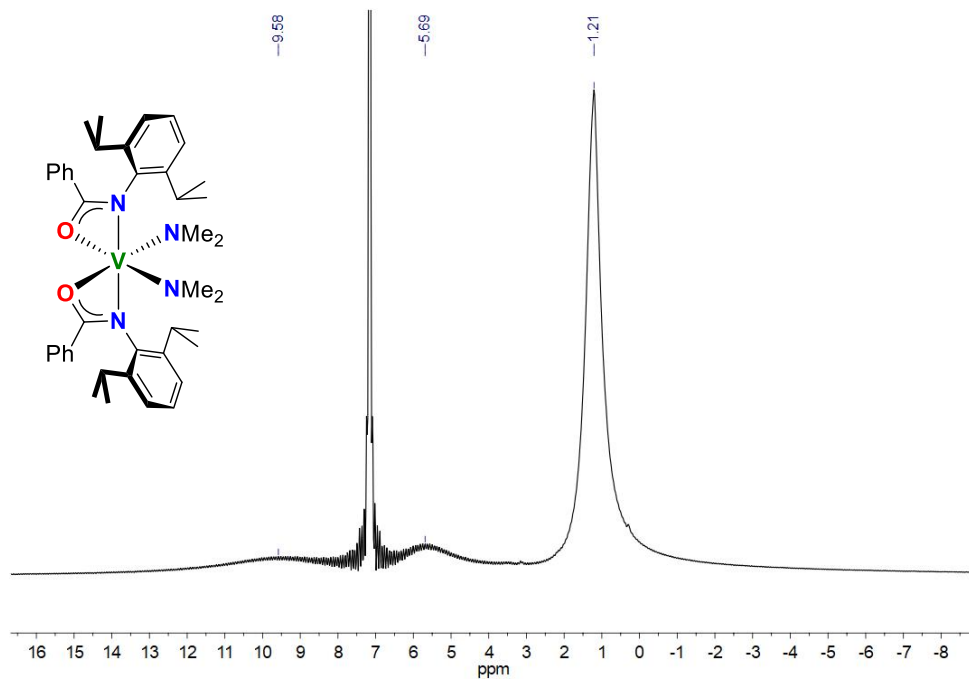
Figure S10. ^{1}H NMR spectrum of **6** and pyrroline *in situ* (C$_6$D$_6$, 300 MHz, 298 K).[2] Broadened resonances result from the paramagnetic V centre.
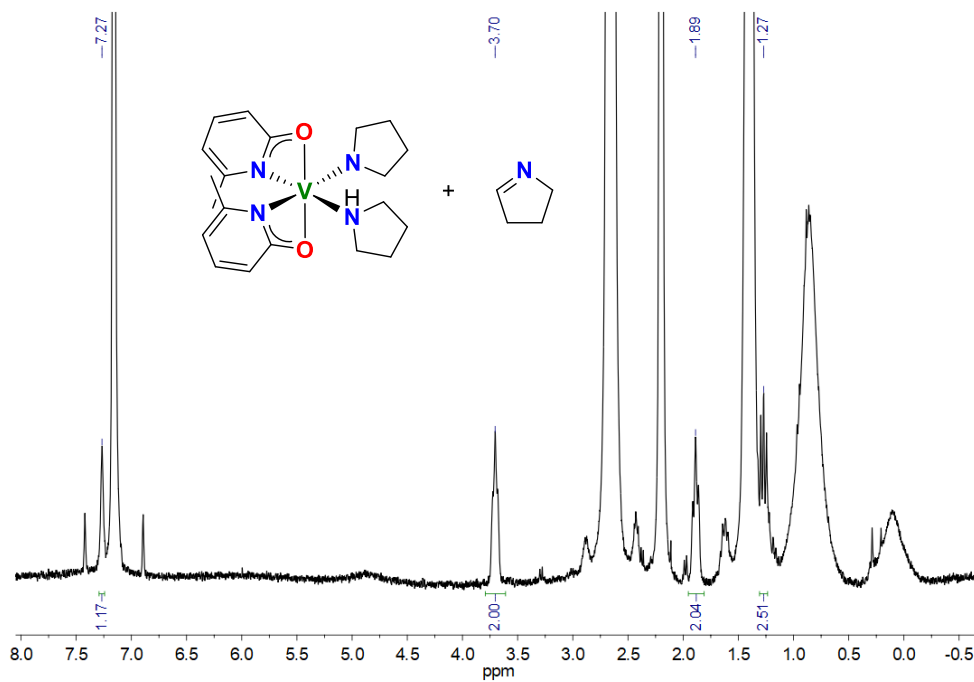
Crystallographic Details

A summary of the crystallographic data for compounds **3**, **4**, **5a-c**, **6**, **7**, **9**, **13**, and **11** is shown in Table S1. The automatic data collection strategy was determined using *COSMO* and the cell determination and integration processes were carried out using *SAINT*. Using *Olex2*,[3] the structures were solved with the *ShelXT*[4] structure solution program using Intrinsic Phasing and the structures were refined using the *ShelXL*[5] refinement package using the Least Squares method. The crystals of complex **4** were found to undergo a phase change and crack at 90 K, thus the data was collected at 120 K to avoid cracking during data collection. However, this had no detrimental effect on the quality of the data. Complex **6** was poorly-diffracting, resulting in relatively poor resolution. This could not be improved to resolve the B-alert in the checkCIF for **6**, although the model still refined well. In the crystal structure of complex **9**, some of the toluene molecules present in the lattice were modelled, but others were highly disordered and could not be modelled; these disordered toluene molecules were removed using the *Olex2* solvent mask command. Additionally, the checkCIF for complex **9** produces a B-alert as the coordinates do not form a properly connected set. Unfortunately, this alert could not be resolved as the structure sits on a symmetry element with half a molecule in the asymmetric unit.

CCDC 2062838-2062846 and 2119611 contain the supplementary crystallographic data for this paper. These data are provided free of charge by The Cambridge Crystallographic Data Centre.

Crystallographic tables:

Table S1. List of crystallographic parameters for compounds **3**, **4**, **5a-c**, **6**, **7**, **9**, **13**, and **11**.

Compound	**3**	**4**
Empirical formula	$C_{20}H_{25}N_4O_3V$	$C_{25}H_{28}N_5O_3V$
Formula weight	420.38	497.46
Temperature/K	100	120
Crystal system	triclinic	triclinic
Space group	P-1	P-1
a/Å	8.9979(5)	8.1620(10)
b/Å	9.5099(6)	9.0032(11)
c/Å	12.4283(8)	16.663(2)
α/°	83.967(2)	86.475(4)
β/°	80.205(2)	81.945(4)
γ/°	78.645(2)	86.385(4)
Volume/Å^3	1024.64(11)	1208.3(3)
Z	2	2
ρ_{calc}g/cm^3	1.363	1.367
μ/mm^{-1}	0.512	0.447
F(000)	440.0	520.0
Crystal size/mm^3	$0.3 \times 0.15 \times 0.14$	$0.28 \times 0.27 \times 0.09$
Radiation	MoKα ($\lambda = 0.71073$)	MoKα ($\lambda = 0.71073$)
2Θ range for data collection/°	3.334 to 59.434	2.472 to 61.112
Index ranges	$-12 \leq h \leq 12, -13 \leq k \leq 13, -17 \leq 1 \leq 17$	$-11 \leq h \leq 11, -12 \leq k \leq 12, -23 \leq l \leq 23$
Reflections collected	10140	30734
Independent reflections	5809 [$R_{int} = 0.0247$, $R_{sigma} = 0.0371$]	7395 [$R_{int} = 0.0309$, $R_{sigma} = 0.0284$]
Data/restraints/parameters	5809/0/258	7395/0/312
Goodness-of-fit on F^2	1.073	0.947
Final R indexes [I>=2σ (I)]	$R_1 = 0.0419$, $wR_2 = 0.1097$	$R_1 = 0.0331$, $wR_2 = 0.1134$
Final R indexes [all data]	$R_1 = 0.0518$, $wR_2 = 0.1149$	$R_1 = 0.0406$, $wR_2 = 0.1223$
Largest diff. peak/hole / e Å^{-3}	0.59/-0.37	0.46/-0.29

Compound	**5a**	**5b**
Empirical formula	$C_{16}H_{24}N_4O_2V$	$C_{16}H_{24}N_4O_2V$
Formula weight	355.33	355.33
Temperature/K	100	100
Crystal system	monoclinic	triclinic
Space group	$P2_1/n$	P-1
a/Å	7.6250(9)	8.9184(5)
b/Å	29.317(4)	9.1750(5)
c/Å	8.7682(10)	11.3271(6)
α/°	90	77.6800(10)
β/°	111.566(6)	87.3910(10)
γ/°	90	89.4980(10)
Volume/Å^3	1822.9(4)	904.57(9)
Z	4	2
ρ_{calc}g/cm^3	1.295	1.305
μ/mm^{-1}	0.558	0.562
F(000)	748.0	374.0
Crystal size/mm^3	$0.21 \times 0.11 \times 0.06$	$0.31 \times 0.2 \times 0.14$
Radiation	MoKα ($\lambda = 0.71073$)	MoKα ($\lambda = 0.71073$)
2Θ range for data collection/°	2.778 to 51.304	3.684 to 61.13
Index ranges	$-7 \leq h \leq 9$, $-29 \leq k \leq 35$, $-10 \leq l \leq 9$	$-12 \leq h \leq 12$, $-13 \leq k \leq 13$, $-16 \leq l \leq 16$
Reflections collected	11780	22197
Independent reflections	3434 [$R_{int} = 0.0614$, $R_{sigma} = 0.0735$]	5531 [$R_{int} = 0.0303$, $R_{sigma} = 0.0274$]
Data/restraints/parameters	3434/0/214	5531/0/214
Goodness-of-fit on F^2	1.019	1.062
Final R indexes [I>=2σ (I)]	$R_1 = 0.0540$, $wR_2 = 0.1098$	$R_1 = 0.0321$, $wR_2 = 0.0801$
Final R indexes [all data]	$R_1 = 0.0876$, $wR_2 = 0.1219$	$R_1 = 0.0392$, $wR_2 = 0.0840$
Largest diff. peak/hole / e Å^{-3}	0.36/-0.30	0.48/-0.38

Compound	5c	6
Empirical formula	$C_{14}H_{20}N_4O_2V$	$C_{20}H_{29}N_4O_2V$
Formula weight	327.28	408.41
Temperature/K	100	100
Crystal system	monoclinic	monoclinic
Space group	$P2_1/c$	$P2_1/n$
a/Å	8.7947(4)	9.5832(7)
b/Å	12.8162(5)	12.8300(9)
c/Å	14.5558(6)	16.4657(12)
α/°	90	90
β/°	105.5090(10)	102.278(4)
γ/°	90	90
Volume/Å^3	1580.91(12)	1978.2(2)
Z	4	4
ρ_{calc}g/cm^3	1.375	1.371
μ/mm^{-1}	0.637	0.524
F(000)	684.0	864.0
Crystal size/mm^3	$0.15 \times 0.11 \times 0.07$	$0.15 \times 0.1 \times 0.05$
Radiation	MoKα ($\lambda = 0.71073$)	MoKα ($\lambda = 0.71073$)
2Θ range for data collection/°	4.306 to 61.042	4.06 to 47.75
Index ranges	$-12 \leq h \leq 12, -18 \leq k \leq 15, -13 \leq 1 \leq 20$	$-10 \leq h \leq 10, -14 \leq k \leq 14, -18 \leq l \leq 18$
Reflections collected	23754	15217
Independent reflections	4820 [$R_{int} = 0.0416$, $R_{sigma} = 0.0355$]	3048 [$R_{int} = 0.0973$, $R_{sigma} = 0.0808$]
Data/restraints/parameters	4820/0/194	3048/0/246
Goodness-of-fit on F^2	1.036	0.958
Final R indexes [I>=2σ (I)]	$R_1 = 0.0316$, w$R_2 = 0.0727$	$R_1 = 0.0520$, w$R_2 = 0.1346$
Final R indexes [all data]	$R_1 = 0.0460$, w$R_2 = 0.0791$	$R_1 = 0.0959$, w$R_2 = 0.1603$
Largest diff. peak/hole / e Å^{-3}	0.50/-0.31	0.28/-0.33

Compound	**7**	**9**
Empirical formula	$C_{24}H_{38}N_5O_2V$	$C_{40}H_{40.57}N_{2.57}O_{2.57}V_{0.86}$
Formula weight	479.53	642.12
Temperature/K	90	90
Crystal system	triclinic	monoclinic
Space group	P-1	C2/c
a/Å	9.1787(4)	27.9809(19)
b/Å	10.7455(5)	18.6624(13)
c/Å	13.7121(6)	47.284(3)
α/°	67.9103(11)	90
β/°	79.1333(11)	94.0449(10)
γ/°	80.9407(12)	90
Volume/Å^3	1225.10(10)	24630(3)
Z	2	28
ρ_{calc}g/cm^3	1.300	1.212
μ/mm^{-1}	0.435	0.285
F(000)	512.0	9488.0
Crystal size/mm^3	$0.18 \times 0.18 \times 0.08$	$0.18 \times 0.14 \times 0.13$
Radiation	MoKα (λ = 0.71073)	MoKα (λ = 0.71073)
2Θ range for data collection/°	3.238 to 61.074	2.626 to 50.808
Index ranges	-13 $\leq$ h $\leq$ 13, -15 $\leq$ k $\leq$ 15, -19 $\leq$ l $\leq$ 19	-33 $\leq$ h $\leq$ 33, -22 $\leq$ k $\leq$ 22, -57 $\leq$ l $\leq$ 57
Reflections collected	29777	129460
Independent reflections	7494 [R_{int} = 0.0278, R_{sigma} = 0.0279]	22644 [R_{int} = 0.0658, R_{sigma} = 0.0489]
Data/restraints/parameters	7494/0/295	22644/0/1479
Goodness-of-fit on F^2	0.969	1.071
Final R indexes [I>=2σ (I)]	R_1 = 0.0368, wR_2 = 0.1154	R_1 = 0.0530, wR_2 = 0.1451
Final R indexes [all data]	R_1 = 0.0495, wR_2 = 0.1283	R_1 = 0.0781, wR_2 = 0.1593
Largest diff. peak/hole / e Å^{-3}	0.46/-0.34	1.49/-0.63

Compound	**13**	**11**
Empirical formula	$C_{42}H_{56}N_4O_2V$	$C_{45}H_{48}N_3O_3V$
Formula weight	699.84	729.80
Temperature/K	100	100
Crystal system	monoclinic	monoclinic
Space group	$P2_1/c$	$P2_1/c$
a/Å	13.2954(10)	13.9174(3)
b/Å	30.480(2)	12.5107(2)
c/Å	10.2846(8)	23.1488(5)
α/°	90	90
β/°	108.269(4)	98.0650(10)
γ/°	90	90
Volume/Å^3	3957.6(5)	3990.72(14)
Z	4	4
ρ_{calc}g/cm^3	1.175	1.215
μ/mm^{-1}	0.289	0.291
F(000)	1500.0	1544.0
Crystal size/mm^3	$0.44 \times 0.11 \times 0.08$	$0.21 \times 0.08 \times 0.06$
Radiation	MoKα ($\lambda = 0.71073$)	MoKα ($\lambda = 0.71073$)
2Θ range for data collection/°	3.492 to 48.368	3.708 to 58.388
Index ranges	$-15 \le h \le 15$, $-35 \le k \le 35$, $-11 \le 1 \le 11$	$-19 \le h \le 19$, $-17 \le k \le 11$, $-31 \le 1 \le 31$
Reflections collected	24373	50659
Independent reflections	6264 [$R_{int} = 0.0569$, $R_{sigma} = 0.0634$]	10770 [$R_{int} = 0.0464$, $R_{sigma} = 0.0410$]
Data/restraints/parameters	6264/0/454	10770/0/490
Goodness-of-fit on F^2	1.093	1.008
Final R indexes [I>=2σ (I)]	$R_1 = 0.0786$, $wR_2 = 0.1563$	$R_1 = 0.0416$, $wR_2 = 0.0932$
Final R indexes [all data]	$R_1 = 0.1156$, $wR_2 = 0.1677$	$R_1 = 0.0696$, $wR_2 = 0.1057$
Largest diff. peak/hole / e Å^{-3}	0.32/-0.44	0.33/-0.37

Figure S11. ORTEP representation of complex **3** with ellipsoids shown at 50% probability and hydrogen atoms (except for the N–H) omitted for clarity. Selected bond lengths (Å) and angles (°): V1–N1, 2.1972(13); V1–O1, 2.0463(11); V1–N4, 2.1885(13).
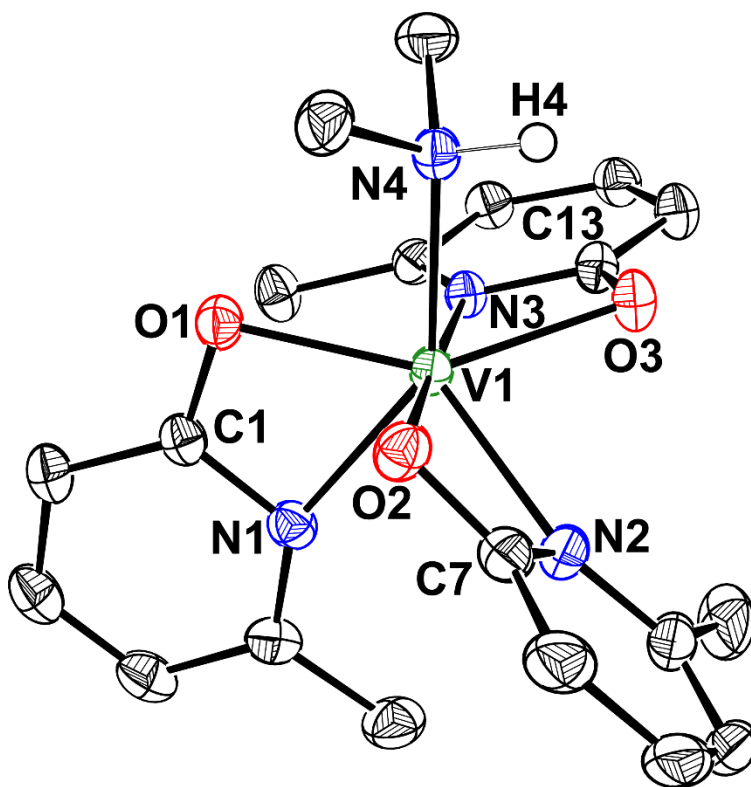
Figure S12. ORTEP representation of complex **4** with ellipsoids shown at 50% probability and hydrogen atoms omitted for clarity. Selected bond lengths (Å) and angles (°): V1–N1, 2.2350(10); V1–O1, 2.0694(9); V1–N4, 2.1066(10).
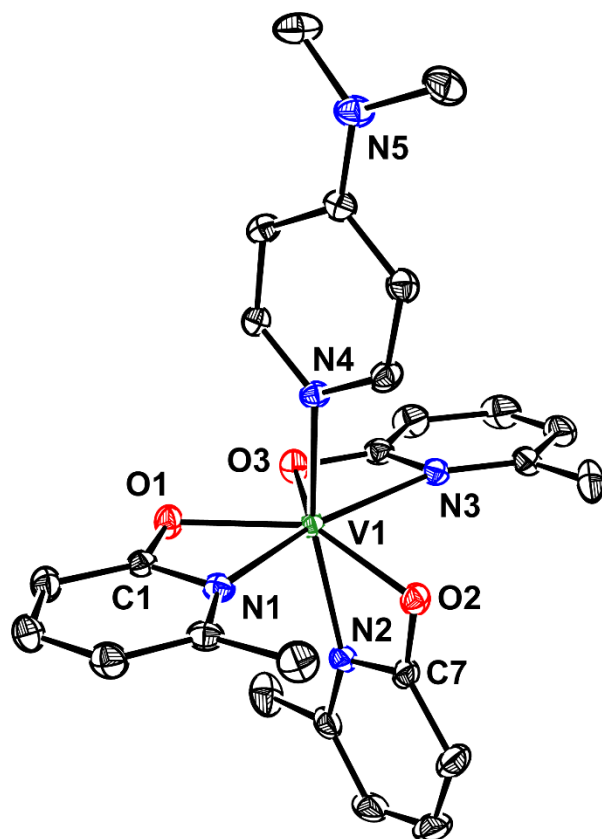
Figure S13. ORTEP representation of complex **5a** with ellipsoids shown at 50% probability and hydrogen atoms and $N(^{i}Pr)_2$ omitted for clarity. Selected bond lengths (Å) and angles (°): V1–N1, 2.253(3); V1–O1, 2.005(2); O1–V1–O2, 150.79(9).
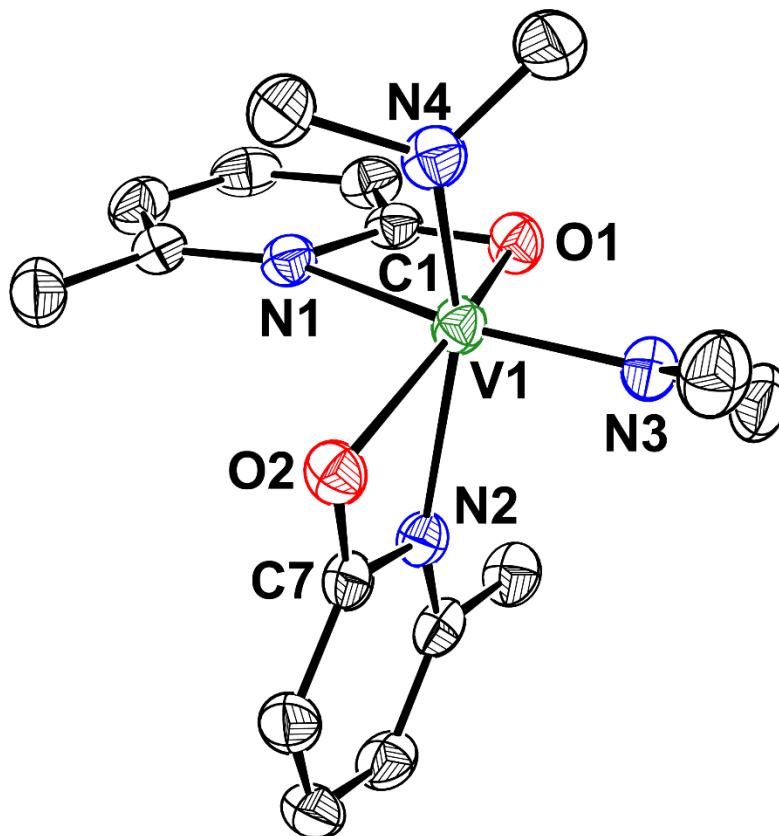
Figure S14. ORTEP representation of complex **5b** with ellipsoids shown at 50% probability and hydrogen atoms omitted for clarity. Selected bond lengths (Å) and angles (°): V1–N1, 2.2169(10); V1–O1, 2.0063(9); O1–V1–O2, 145.82(4).
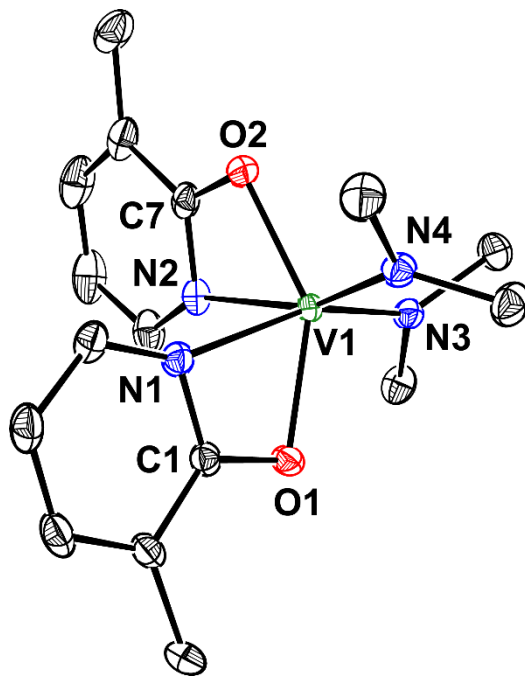
Figure S15. ORTEP representation of complex **5c** with ellipsoids shown at 50% probability and hydrogen atoms omitted for clarity. Selected bond lengths (Å) and angles (°): V1–N1, 2.2118(12); V1–O1, 2.0125(9); O2–V1–O1, 145.26(4).
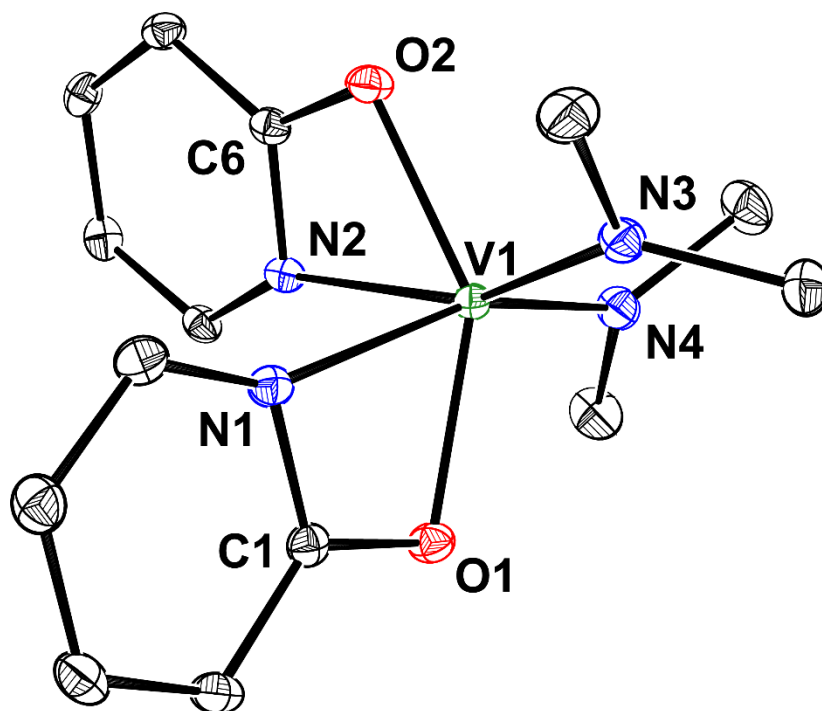
Figure S16. ORTEP representation of complex **6** with ellipsoids shown at 50% probability and hydrogen atoms (except for N–H) omitted for clarity. Selected bond lengths (Å) and angles (°): V1–N1, 2.225(4); V1–O1, 2.061(3); V1–N3, 1.891(4); V1–N4, 2.193(4).
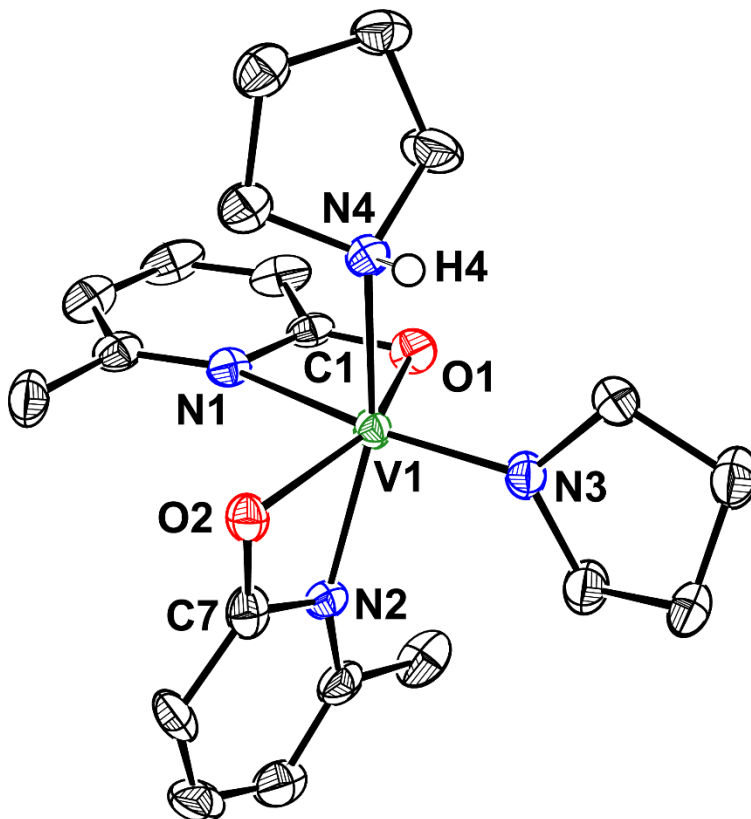
Figure S17. ORTEP representation of complex **7** with ellipsoids shown at 50% probability and hydrogen atoms (except for N–H) omitted for clarity. Selected bond lengths (Å) and angles (°): V1–N1, 2.2125(11); V1–O1, 2.1267(9); V1–O2, 2.0207(9); V1–N3, 2.1781(10); V1–N4, 2.1799(11); V1–N5, 1.8755(11); C7–O2–V1, 136.24(9).
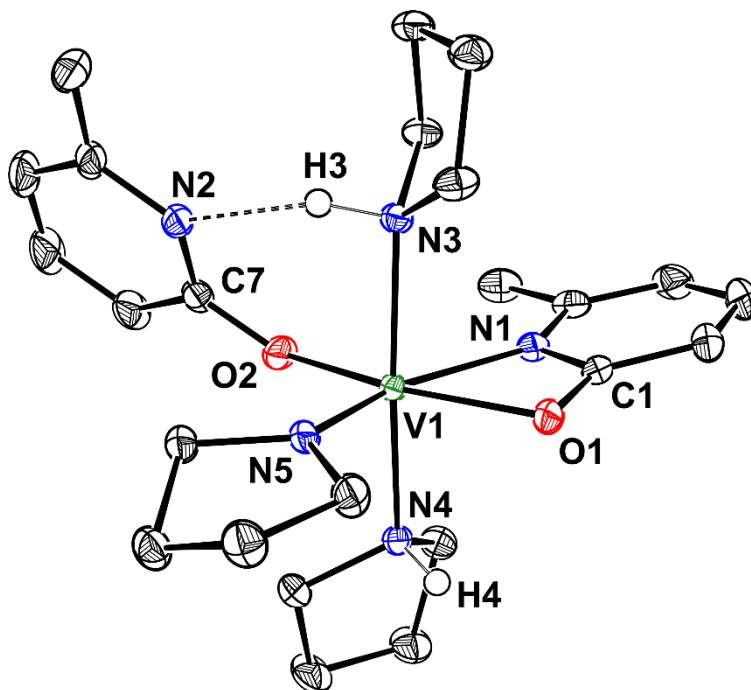
Figure S18. ORTEP representation of complex **9** with ellipsoids shown at 50% probability and mesityl groups and hydrogen atoms omitted for clarity (top). The structure including mesityl groups is shown as well (bottom). Selected bond lengths (Å) and angles (°)**:** V1–N1, 2.141(2); V1–O1, 2.0436(18); V1–N4, 2.117(2); V2–O2, 1.9322(18); C6−O2−V2, 161.34(18).
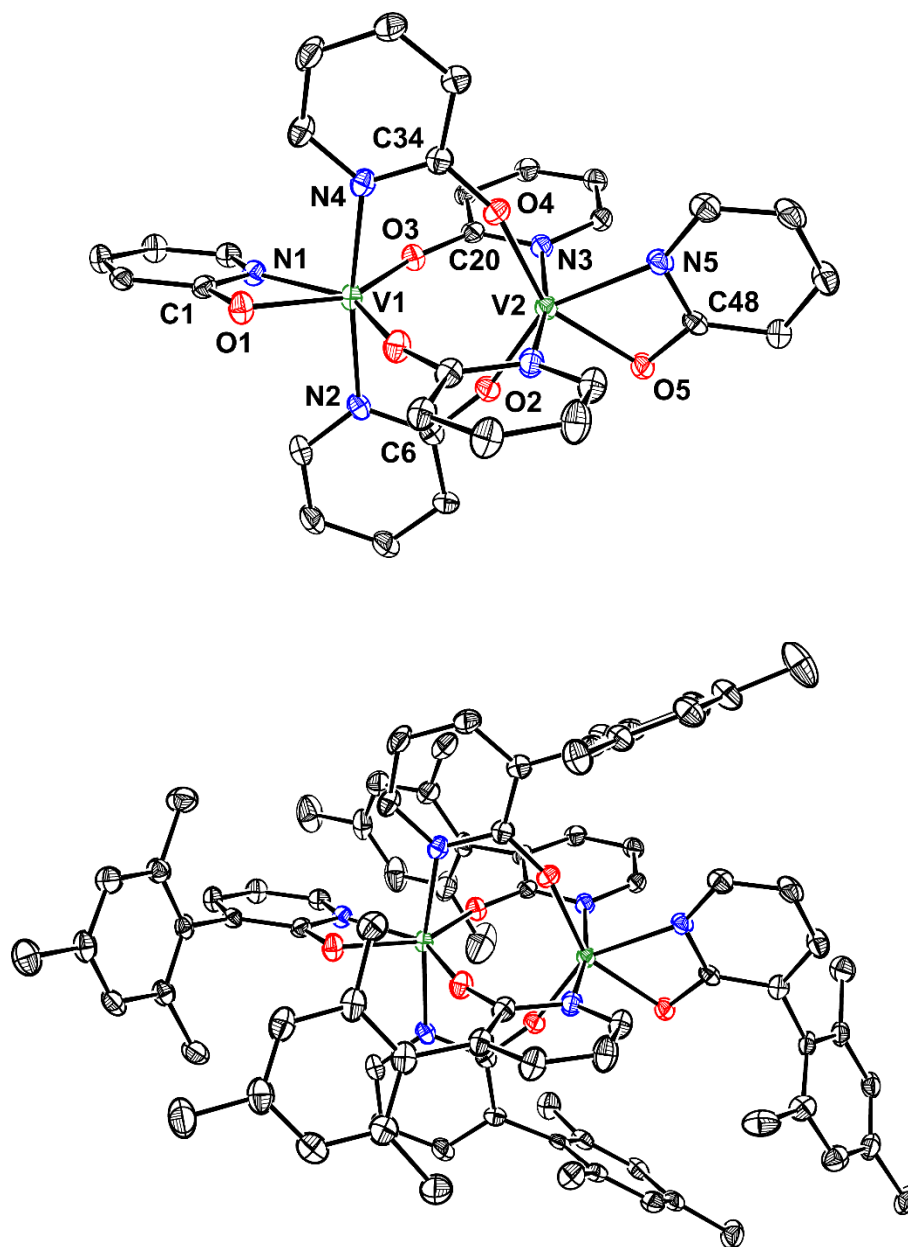
Figure S19. ORTEP representation of complex **13** with ellipsoids shown at 50% probability and hydrogen atoms omitted for clarity. Selected bond lengths (Å) and angles (°): V1–O1, 2.154(3); V1–N1, 2.072(4); V1–N4, 1.859(4); N1–V1–N2, 145.38(16).
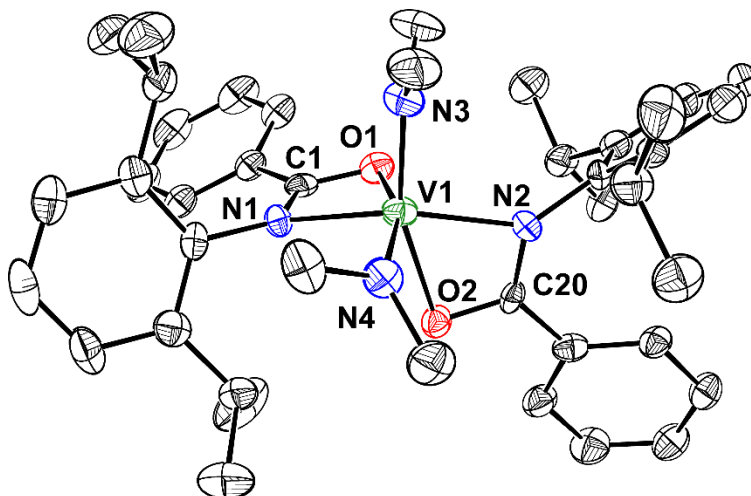
Figure S20. ORTEP representation of complex **11** with ellipsoids shown at 50% probability and hydrogen atoms omitted for clarity. Selected bond lengths (Å) and angles (°): V1–N1, 2.1512(14); V1–O1, 2.0081(11); V1–N2, 2.1215(13); V1–O2, 1.9536(11); V1–N3, 2.0936(13); V1–O3, 1.9550(12); O2–V1–N2, 65.90(5).
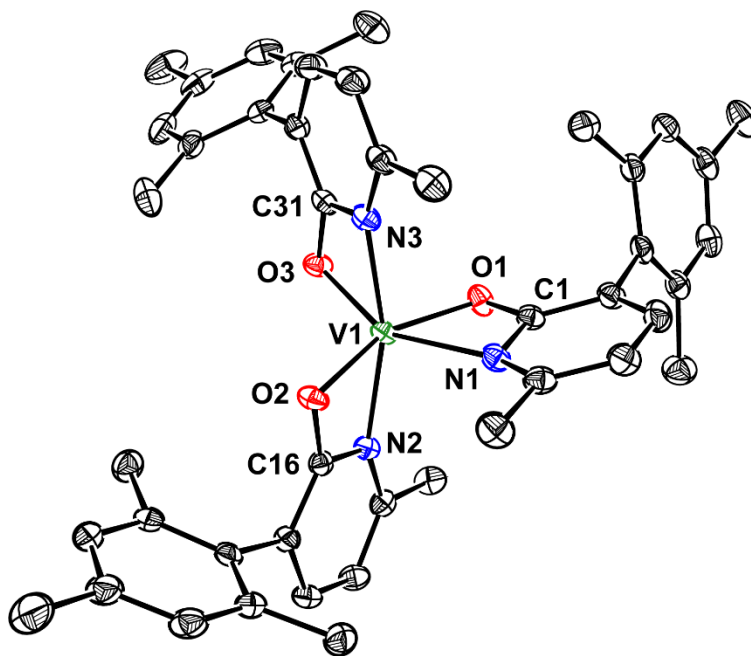
Computational Data

The spin density plots for the paramagnetic computed structures are shown below. The coordinates for all computed structures can be found in the combined .xyz file provided as supplementary information.

Figure S21. Spin density plot of complex **5a** (spin density = cyan, isovalue = 0.01).
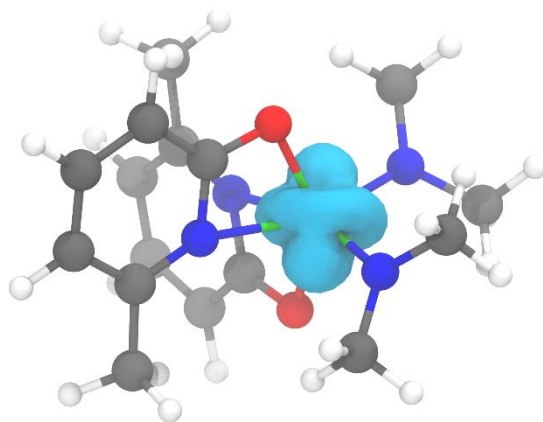
Figure S22. Spin density plot of complex **5b** (spin density = cyan, isovalue = 0.01).
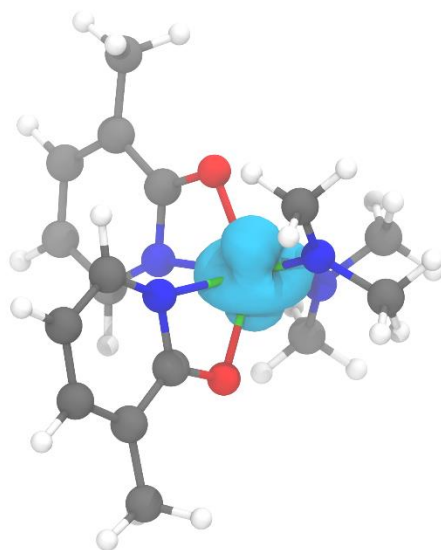
Figure S23. Spin density plot of complex **5c** (spin density = cyan, isovalue = 0.01).
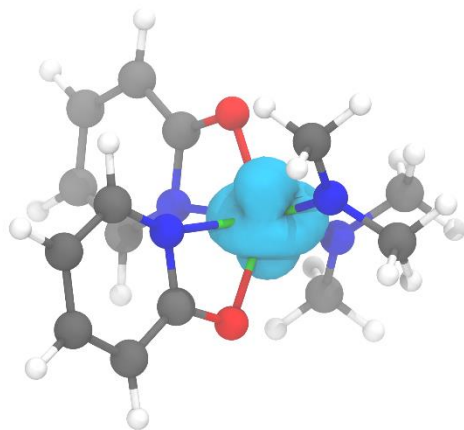
Figure S24. Spin density plot of complex **3** (spin density = cyan, isovalue = 0.01).
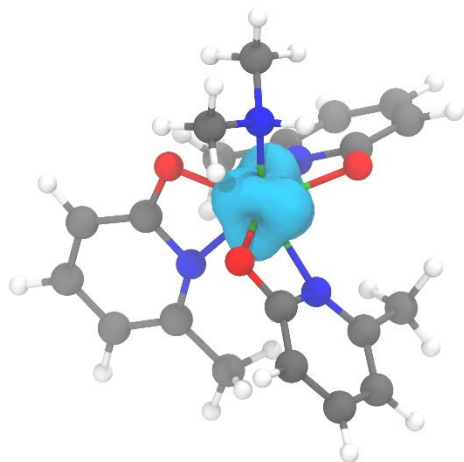
Table S2. Thermochemical comparison of the two possible spin states for V(III) complex **3**.

Spin State	Electronic Energy (EE) (Hartrees)	Thermal Free Energy Correction (Hartrees)	EE + Thermal Free Energy Correction (Hartrees)	EE + Thermal Free Energy Correction (kcal/mol)	Relative Free Energy (kcal/mol)
triplet ($S = 1$)	−2166.576438	0.368611	−2166.207827	−1359315.990	0.0
singlet ($S = 0$)	−2166.521597	0.369066	−2166.152531	−1359281.292	34.7

Thus, the triplet spin state of complex **3** is much more energetically favourable compared to the singlet spin state.

References

(1)   S. E. Griffin and L. L. Schafer, *Inorg. Chem.*, 2020, **59**, 5256–5260.

(2)   H. Poisel, *Monatshefte für Chemie*, 1978, **109**, 925–928.

(3)   O. V. Dolomanov, L. J. Bourhis, R. J. Gildea, J. A. K. Howard and H. Puschmann, *J. Appl. Cryst.,* 2009, **42**, 339.

(4)   G. M. Sheldrick, *Acta Cryst. Sect. A,* 2015, **71**, 3.

(5)   G. M. Sheldrick, *Acta Cryst. Sect. C,* 2015, **71**, 3.